Available online at www.sciencedirect.com
SCIENCE DIRECT®
Coordination Chemistry Reviews 249 (2005) 1609–1619
COORDINATION CHEMISTRY REVIEWS
www.elsevier.com/locate/ccr

Review

Structure–function relationships of nickel–iron sites in hydrogenase and a comparison with the active sites of other nickel–iron enzymes

Anne Volbeda, Juan C. Fontecilla-Camps *

Laboratoire de Cristallographie et de Cristallogenèse des Protéines, Institut de Biologie Structurale J.P. Ebel (CEA-CNRS-UJF), 41 rue Jules Horowitz, 38027 Grenoble Cédex 1, France

Received 25 October 2004; accepted 10 December 2004
Available online 12 April 2005

Contents

Abstract

Recent studies of [NiFe]-hydrogenases have provided a significant amount of new structural and kinetic data on the many states the active site displays upon enzyme inhibition, its activation and during catalysis. Other Ni–Fe containing active sites have been found in the bifunctional carbon monoxide dehydrogenase/acetyl coenzyme A synthase that is involved in anaerobic carbon fixation through the Wood–Ljungdahl pathway. Here, we discuss the influence of the protein environment on the reactivity of these three active sites and analyze the differences and similarities in their structural and chemical properties.

Keywords: Hydrogenase; Nickel–iron–sulfur clusters; Gas metabolism; Carbon monoxide dehydrogenase; Acetyl coenzyme A synthase

1. Introduction

Several NiFeS clusters found in enzyme active sites resemble natural minerals like greigite ($NiFe_5S_8$), which may have played a crucial role in the emergence of life ([1] and references therein). Such mineral systems catalyze, for example, the formation of peptides from amino acids in extreme environments such as geothermal vents [2]. During evolution, incorporation of similar, sometimes only slightly modified clusters in a protein matrix has lead to a better-controlled and more efficient catalysis. Here, we focus on the NiFe containing active sites of [NiFe] hydrogenase and compare these with NiFe active sites in carbon monoxide dehydrogenase (CODH) and acetyl coenzyme A synthase (ACS).

[NiFe]-hydrogenases play an essential role in the energy metabolism of numerous microorganisms by catalyzing the

Abbreviations: EPR, electron paramagnetic resonance; FT-IR, Fourier transform infrared; XAS, X-ray absorption spectroscopy; EXAFS, extended X-ray absorption fluorescence spectroscopy; DFT, density functional theory; ENDOR, electron nuclear double resonance; ESEEM, electron spin echo envelope modulation

* Corresponding author. Tel.: +33 4 38 78 59 20; fax: +33 4 38 78 51 22.
E-mail address: juan.fontecilla@ibs.fr (J.C. Fontecilla-Camps).

0010-8545/$ – see front matter © 2004 Elsevier B.V. All rights reserved.
doi:10.1016/j.ccr.2004.12.009

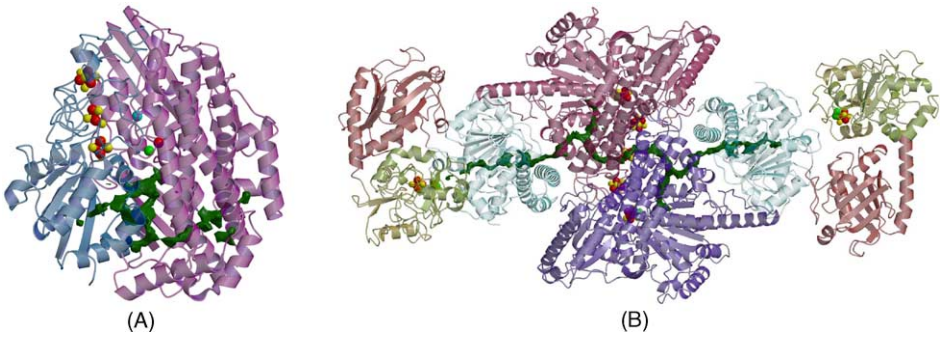

Fig. 1. Polypeptide folds of (A) *Desulfovibrio gigas* [NiFe]-hydrogenase (pdb code 2FRV) and (B) *Moorella thermoacetica* carbon monoxide dehydrogenase/acetyl coenzyme A synthase (CODH/ACS, pdb code 1OAO). The large and the small subunit of the hydrogenase are shown in violet and blue, respectively. The two CODH subunits and the three domains of the two ACS subunits are depicted in pink, violet, light-blue, orange and yellow, respectively. Gas accessible tunnels are shown in dark-green. Ni, Fe, Mg and S atoms are shown as spheres that are colored green, red, light-blue and yellow, respectively.

heterolytic cleavage of molecular hydrogen, according to the reaction:

$$H_2 \Leftrightarrow H^- + H^+ \Leftrightarrow 2e^- + 2H^+ \quad (1)$$

(for recent reviews see [3–8]). In spite of the apparent simplicity of this reaction, a large number of both inhibited and active states have been characterized in these highly complex enzymes. [NiFe]-hydrogenases have been classified in four classes, according to sequence similarity, subunit composition, cellular location and function. They can also be classified as either H_2 uptake, H_2 evolving, or bidirectional enzymes and as H_2 sensors [4,5,9]. So far, crystal structures have only been reported for a few H_2 uptake hydrogenases [10–18]. These are all composed of a small subunit carrying three FeS clusters and a large subunit that contains the Ni–Fe active site (Fig. 1A). Along with Fe-only hydrogenases [19] they are the only enzymes that contain both CO and CN^- in their active site. Incorporation to [NiFe] enzymes of both these usually toxic molecules and the metal ions requires complex pathways involving fairly well-characterized proteins [20].

The aim of this review is to analyze the most recent spectroscopic, electrochemical and kinetic data concerning standard H_2 uptake [NiFe] hydrogenases in the context of already available structural information. In addition, a comparison is made with the Ni–Fe active sites of carbon monoxide dehydrogenase (CODH) and acetyl coenzyme A synthase (ACS). Although the three enzymes catalyze different reactions and have completely different structures (Fig. 1), they are all involved in gas-based processes and have a similar coordination of the catalytic nickel ion. A main goal is to determine how the differences in active site structures and their respective protein environments determine the specificity of the reaction.

2. Nickel–iron hydrogenases

2.1. Structural description

High-resolution X-ray crystal structures have been obtained for five [NiFe] hydrogenases purified from closely

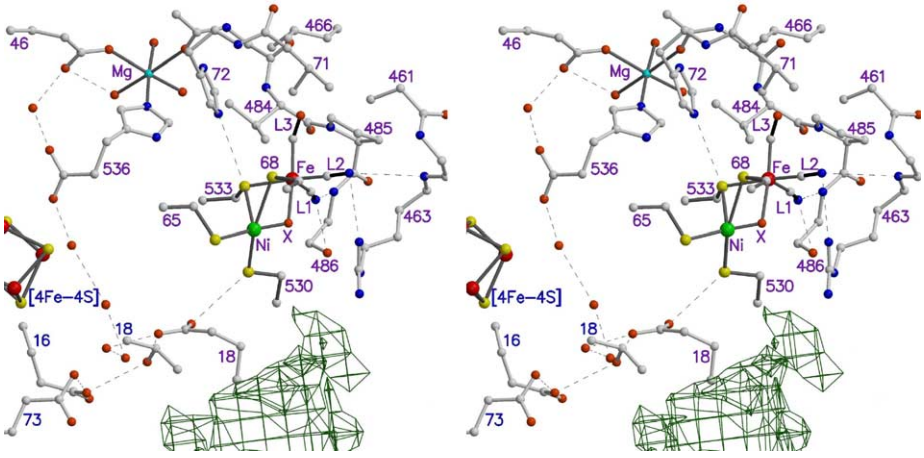

Fig. 2. Stereo pair showing part of the active site environment of oxidized *D. gigas* [NiFe]-hydrogenase (same view as in Fig. 1A.Used color code: Ni green, Fe red, Mg light-blue, S yellow, O orange-red, N dark-blue and C white. Dashed lines indicate putative H-bonds. A gas-accessible tunnel region is highlighted as a dark-green grid. Residues are labeled in violet and blue for the large and small subunit, respectively. X is a Ni-Fe bridging ligand that has been modeled as an O-atom.

related sulfate-reducing bacteria; *Desulfovibrio* (*D.*) *gigas* [10,11], *D. vulgaris* (Miazaki) [12–14], *D. fructosovorans* [15,16] and *D. desulfuricans* [17], and from *Desulfomicrobium* (*Dm.*) *baculatum* [18]. A common feature of the active site structures is the presence of one nickel and one iron ion bridged by two cysteine ligands (Fig. 2). The nickel ion is further coordinated by two terminal cysteine ligands, one of which is substituted by seleno-cysteine in the *Dm. baculatum* enzyme. The iron ion is bound by three additional diatomic ligands. The protein environment is virtually identical in the five enzymes of known structures and it is highly conserved in all [NiFe]-hydrogenases for which amino acid sequence data are available.

The Ni–Fe site is completely buried close to the center of the enzyme, at about 30 Å from the surface. Consequently, specific pathways should exist for molecular hydrogen, electrons and protons. A hydrophobic tunnel points at an empty Ni-coordination site, opposite to the apical S_{533} ligand that is hydrogen-bonded to the side chain of His72. Access of small gas molecules to the active site should be favored by this tunnel. The three FeS clusters of the small subunit define an electron transfer pathway between the Ni and the surface with typical center-to-center distances between successive redox centers of about 12 Å (see also Fig. 1A). The Mg^{2+} site at the C-terminus of the large sub-unit (which is replaced by Fe in the *Dm. baculatum* enzyme [18]) may be involved in a proton transfer pathway comprising, in that order, Cys530, Glu18, four internal water molecules, the C-terminal carboxylate of His536, another internal water molecule, Glu46 and a water ligand of Mg, located close to the molecular surface [3]. A second series of hydrogen bonds extending beyond Glu18 involves Thr18, Glu16 and Glu73 from the small subunit (see Fig. 2). Taken together, the two regions define a putative pathway that might couple rapid electron and proton transfer between the active site and the proximal cluster (see also chapters 6 and 8 in [4]). Along these lines, it has been determined that its redox midpoint potential is pH-dependent [21], indicating that reduction of the cluster is most probably accompanied by a protonation event, possibly involving Glu73. Other pathways for proton transfer may also exist [17].

When [NiFe] hydrogenases are purified under air, the resulting oxidized preparations usually display two EPR signals called Ni-A and Ni-B. The corresponding states are both inactive but show very different activation properties when treated anaerobically with H_2 or other reducing agents like dithionite. The Ni-A state requires hours of such reductive treatment before it is fully converted to active enzyme, which then displays the so-called Ni-C EPR signal. On the other hand, the Ni-B state activates within minutes. Accordingly, Ni-A, Ni-B and Ni-C have respectively been called unready, ready and active states of the enzyme [22,23]. Based on their EPR spectra, they have been assigned to paramagnetic Ni(III) species [24,25]. One-electron reductions of Ni-A, Ni-B and Ni-C result in EPR-silent Ni(II) intermediates that have been called Ni-SU (for Silent Unready), Ni-SI (SIlent ready) and Ni-R (fully Reduced and active), respectively [3]. An alternative nomenclature that is widely used in the literature is given in Table 2.

2.2. Crystallographically characterized structures of the Ni–Fe active site

FT-IR studies have shown that the active site diatomic ligands correspond to one CO and two CN^- molecules (Fig. 3) [26–28]. In the initially published 1.8 Å resolution structure of the *D. vulgaris* (Miazaki) enzyme [12] one of the diatomic ligands was modeled as SO. However, in subsequent structures obtained at 1.4–1.2 Å resolution [14] the authors modeled the three ligands as CO, which is *iso*-electronic with CN^-. As first observed in the structure of the *D. gigas* enzyme, two of the ligands are located in a hydrophilic environment and establish H-bonding interactions with protein atoms, whereas the third one is entirely surrounded by hydrophobic residues (Fig. 2). Based on these observations, we have assigned the former to CN^- and the latter to CO [27]. Additional crystallographic evidence for this assignment has come from the refinement at 1.8 Å resolution of a mutant of the *D. fructosovorans* enzyme performed with weak distance restraints for the iron ligands. The resulting Fe–CO bond was 1.7 Å long, whereas the CN^- ligands refined to a distance of

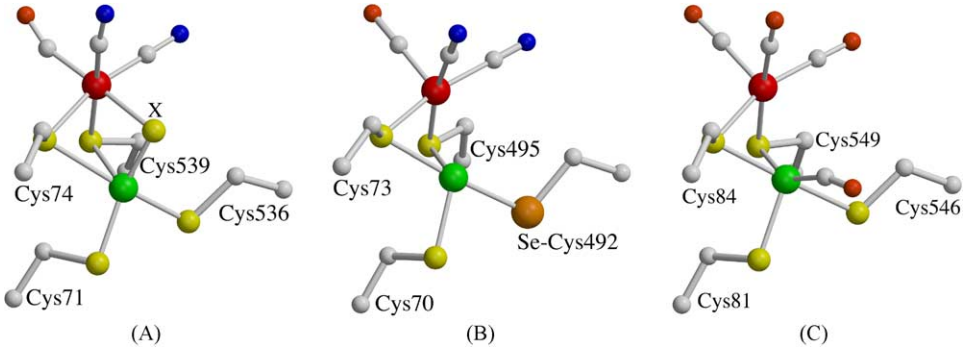

Fig. 3. Ni–Fe active site structures: (A) an oxidized state of the *D. desulfuricans* enzyme, with the bridging ligand X assigned to a 50% occupied S-atom, (B) a reduced state of the *Dm. baculatum* enzyme, which has a natural seleno-cysteine, and (C) a CO complex of the *D. vulgaris* (Miyazaki) enzyme. The respective pdb deposition codes are 1E3D, 1CC1 and 1UBK.

Table 1
Ni–Fe and ligand distances based on crystal structures and on DFT analyses

Organism/model	Enzymatic state	d_{max} (Å)	N_{mol}[a]	Ni–Fe	Ni–S_{65}	Ni–S_{530}	Ni–S_{68}	Ni–S_{533}	Ni-X[b]	Fe–S_{68}	Fe–S_{533}	Fe–X[b]	Fe-L1	Fe-L2	Fe-L3
D. gigas	Oxidized	2.5	6	2.8	2.3	2.3	2.5	2.5	1.8	2.3	2.3	2.2	1.8	1.8	1.7
D. vulgaris (Miyazaki)	Oxidized[c]	1.8	1	2.6	2.2	2.3	2.4	2.4	2.2	2.1	2.4	2.2	2.1	1.8	1.9
D. fructosovorans	Oxidized	1.8	4	2.9	2.2	2.3	2.5	2.5	1.9	2.3	2.3	2.2	2.0	1.9	1.7
D. desulfuricans	Oxidized	1.8	2	2.9	2.2	2.2	2.6	2.5	1.9	2.3	2.3	2.3	1.8	1.9	1.8
Dm. baculatum	Reduced[d]	2.1	1	2.5	2.3	2.5	2.3	2.6	–	2.3	2.4	–	1.9	1.9	1.9
D. vulgaris (Miyazaki)	Reduced[c]	1.4	1	2.6	2.3	2.2	2.3	2.4	-	2.3	2.4	-	2.2	1.9	1.8
D. vulgaris (Miyazaki)	CO complex	1.2	6	2.6	2.3	2.3	2.3	2.3	1.8	2.2	2.3	–	1.9	1.9	1.8
D. vulgaris (Miyazaki)	CO*[e]	1.3	3	2.6	2.3	2.3	2.3	2.4	–	2.3	2.3	–	1.9	2.0	1.7
Selected DFT models:	SI-CO (S = 1)[f]	–	–	2.9	2.3	2.7	2.4	2.4	nr	2.4	2.3	–	1.9	1.9	1.7
	Ni–C[g]	–	–	2.7	2.3	2.3	2.4	2.4	1.7	2.4	2.4	1.7	nr	nr	nr
	Ni-R (S = 0)[h]	–	–	2.5	2.2	2.3	2.3	2.5	1.6	2.3	2.3	1.7	nr	nr	nr
	Ni–R (S = 1)[h]	–	–	2.5	2.4	2.4	2.4	2.3	1.7	2.4	2.4	1.6	nr	nr	nr

nr: not reported.
[a] Number of independent molecules/structures (average distances are given).
[b] Exogenous ligand (O, S, C or H, see text).
[c] L1 assigned as SO ligand.
[d] S_{530} replaced by Se atom.
[e] After photolytic cleavage of CO.
[f] From [32].
[g] From [53].
[h] From [55].

1.9–2.0 Å from Fe [16]. This result is in close agreement with the structure of a small molecule with a $Fe(CN)_2CO$ moiety [29] and with DFT calculations [30,31]. An equivalent refinement of the *D. gigas* enzyme, performed at 2.54 Å resolution using strict six-fold non-crystallographic symmetry gave similar bond lengths for the diatomic ligands [16] (Table 1). A similar distribution of metal-ligand distances after unrestrained refinement at 1.2 Å resolution has been found more recently for the *D. vulgaris* (Miazaki) enzyme [14].

Three kinds of active site structures have, so far, been characterized by X-ray crystallography. In oxidized forms of the enzyme an exogenous ligand bridges the Ni and Fe ions (Fig. 3A). Its identity seems to vary according to the organism and/or the redox state [11,12,16,17]. When the bridging ligand is present the Fe and Ni ions have distorted octahedral and distorted square pyramidal coordination respectively with Cys533 (*D. gigas* numbering) as the apical ligand in the latter. In reduced, active enzymatic states, no electron density has been found for an exogenous ligand, but the conformation of the cysteine ligands suggests that the bridging site is occupied by H^-, a ligand undetectable at the resolution of these crystallographic studies (Fig. 3B) [13,18]. The presence of a bridging H^- would again result in square pyramidal Ni and octahedral Fe coordinations.

Crystal structures of the enzyme bound with CO have also been published [14]. They show that this competitive inhibitor binds to the vacant terminal Ni site (Fig. 3C), next to the tip of a long hydrophobic tunnel. As discussed further

Table 2
FT-IR bands of diatomic Fe-ligands in 15 Ni–Fe active site intermediates

State of the enzyme[a]	$\nu_{CN,sym}$ (cm^{-1})	$\nu_{CN,asym}$ (cm^{-1})	ν_{CO} (cm^{-1})	State of the enzyme[a]	$\nu_{CN,sym}$ (cm^{-1})	$\nu_{CN,asym}$ (cm^{-1})	ν_{CO} (cm^{-1})
Ni-A (Ni_u*)[b]	2093	2082	1945	Ni-C_I (Ni_a-C*)[c]	2085	2073	1951
Ni-SU (Ni_u-S)[c]	2100	2088	1948	Ni-C_{II} (Ni_a-C*)[c]	2084	2073	1948
Ni-B (Ni_r*)[b]	2090	2079	1943	SI-CO[d] (Ni_a-SCO)	2084	2069	1931
Ni-"S" (Na_2S-treated)[c]	2066	2057	1909	SI-CO_{red}[d] (Ni_a-SCO)	2083	2068	1928
Ni-SI_I (Ni_r-S_{1910})[b]	2067	2052	1910	Ni-R_I (Ni_a-SR_{1913})[c]	2058	2043	1913
Ni-SI_{II} (Ni_r-S_{1931})[c]	2084	2073	1931	Ni-R_{II} (Ni_a-SR_{1921})[c]	2064	2048	1921
Ni-SI_{II} (Ni_a-S_{1931})[c]	2084	2073	1931	Ni-R_{III} (Ni_a-SR_{1936})[c]	2072	2059	1936
Ni-L (Ni_a-L*)[b]	2058	2043	1898				

[a] Alternative nomenclature in parentheses, an asterisk (*) indicates an EPR-detectable state.
[b] From *A. vinosum* [39].
[c] From *A. vinosum* [40].
[d] From *D. fructosovorans* [32].

below, the Ni is probably in a divalent state. If we assume that in this complex the bridging site is not occupied by H^- [32], both the Fe and the Ni have a square pyramidal coordination, which for the latter is significantly distorted. When compared to the other active site structures, Cys533 and Cys65 (*D. gigas* numbering) switch roles as Ni ligands: the former becomes equatorial whereas the latter is apically bound. Upon photolysis of the Ni–CO bond [14] a structure similar to the reduced, active enzyme is obtained with Cys533 occupying again an apical position (Table 1).

Additional information on Ni-ligand interactions has been obtained from XAS studies [33-36]. A range-extended EXAFS analysis of an oxidized preparation of the *D. gigas* enzyme showed one Ni–O bond at 1.91 Å, two Ni–S bonds at ≈2.2 Å and 1–2 additional Ni–S bonds at 2.35 ± 0.05 Å [36]. These values are close to the distances found by X-ray crystallographic analyses for similar enzyme states (Table 1). For the H_2-reduced enzyme, the same authors found that two Ni–S bonds remain at ≈2.2 Å, but that the remaining ones increase to 2.47 ± 0.05 Å. Moreover, a better fit to the experimental data was obtained when a Ni–O interaction at 2.03 Å was included. However, the latter proposition does not agree with the crystal structures.

A former EXAFS study of the *A. vinosum* enzyme [34] suggested the presence of one O-ligand in Ni-A and Ni-B and two O-ligands in Ni-SU, at a distance of ≈1.9 Å from the Ni. No O-ligand was found in the more reduced states of the active site, for which a shortening of the Ni–Fe distance of about 2.9–2.6 Å was proposed. This agrees with the published crystal structures except for the oxidized state of the *D. vulgaris* (Miyazaki) enzyme (Table 1). The number of ligands to the Ni was proposed to decrease at pH 6 from five in Ni-B to four in both Ni-R and a protonated form of Ni-SI called Ni-SI_{II}. The proposal of a six-coordinated Ni(III) in the Ni-C state requires that both the Fe ion and a hydride be included as ligands. A nickel–carbon interaction at 1.78 Å was observed for the EPR-silent CO complex, in excellent agreement with the crystal structures of Higuchi and coworkers [14].

The redox and protonation state of the hydrogenase active site cannot be directly obtained from X-ray crystallography. However, these states need be known before the mechanism of hydrogen bio-catalysis can be fully understood. Consequently, results from other techniques are essential and will be discussed below.

2.3. Recent spectroscopic studies

EPR spectroscopy has been instrumental in detecting and characterizing the various paramagnetic states displayed by [NiFe] hydrogenases. Although a great deal has been learned about these fascinating enzymes using this technique [37], a disadvantage of EPR spectroscopy is that it cannot generally characterize diamagnetic states, except by the absence of a signal. With the observation of intrinsic high-frequency infrared bands for *Allochromatium* (*A.*) *vinosum* [NiFe] hydrogenase [38] that correspond to one CO and two CN-ligands

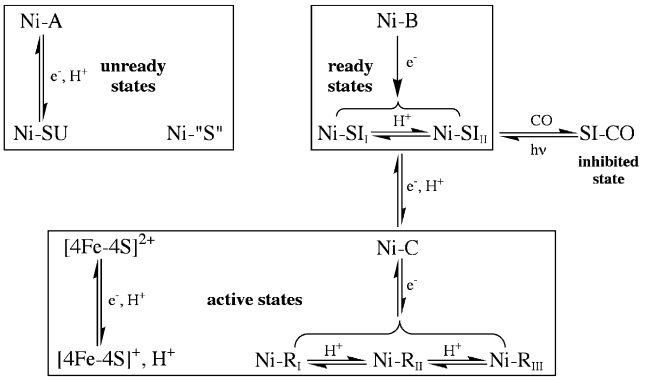

Scheme 1.

[26,28] and the subsequent observation that, as expected, they respond to changes at the active site [11,27,39], the FT-IR technique has allowed the detection of many additional diamagnetic states. In addition, it has provided an independent characterization of the paramagnetic ones. Through a combination of EPR and FT-IR results, at least 13 stable active site forms have been detected [32,40], with additional less-stable ones found only at low temperature (Table 2).

Thus, in a recent FT-IR spectro-electrochemical study of *A. vinosum* [NiFe]-hydrogenase [40], several new active site states were detected and characterized. An EPR-silent unready state was obtained when excess Na_2S was added to enzyme in the Ni-C state at pH 6.5, at room temperature and under Ar. This state, which is called Ni-"S" here, was assigned to an S-bound species, showing a unique set of three IR bands close to those of the Ni-SI_I species, which has one fewer proton than the Ni-SI_{II} state (Scheme 1, Table 2). Two Ni-SI_{II} states with identical spectroscopic properties have been distinguished in the *A. vinosum* enzyme according to their response to H_2: a ready, inactive state at 2 °C and an active one at room or higher temperature [40]. For simplicity only the ready Ni-SI_{II} state is included in Scheme 1.

DFT calculations have suggested that an OH^- ligand bridges the Ni and Fe ions in the Ni-B state [41,42]. If a bridging OH^- were also present in the Ni-SI_I state, as proposed by some authors [40,43], the similarity between its FT-IR spectrum and that of the Na_2S-treated enzyme would be due to a SH^- bridging ligand in the latter. This might correspond to the sulfur bridging ligand postulated in the crystal structures of as-prepared *D. vulgaris* (Miyazaki) and *D. desulfuricans* [NiFe]-hydrogenases [12,17]. However, the presence of a bridging OH^- ligand in both Ni-B and Ni-SI_I is difficult to reconcile with the irreversibility of the reduction of Ni-B at 2 °C and with the observation that the oxidation rate of Ni-SI_I to Ni-B at higher temperature does not depend on the applied potential [44]. It has also been proposed that the putative OH^- ligand in Ni-B leaves the active site upon reduction, remains trapped nearby in the unready Ni-SI states and is finally released upon transition to an active state [42]. Clearly more structural data are needed to clarify these points.

Using the *D. fructosovorans* enzyme, De Lacey et al. reported a kinetic effect in the anaerobic conversion of Ni-SI_I and Ni-SI_{II} to Ni-B when H_2O was replaced by D_2O. Because the kinetics of this reaction are independent of pH, it seems that the rate-limiting step is the incorporation of an OH^- ligand originating from solvent [45]. Along the same lines, the anaerobic oxidation rate of the Ni-SI states in the E25Q mutant was found to be six times slower than the corresponding rate in the native enzyme. In the wild type enzyme the carboxylate group of the glutamic acid (E18 in the *D. gigas* enzyme) may exchange a proton with a terminal cysteine ligand of the Ni (Cys530 in *D. gigas*, see Fig. 2). The slower oxidation rate in the mutant is most likely due to the inability of glutamine to abstract a proton from a water molecule. The mutant has EPR and FT-IR spectra identical to the native enzyme but displays no catalytic activity (except for the *para*-H_2 to *ortho*-H_2 conversion) showing that E25 is crucial for proton transfer reactions occurring during turnover [46].

De Lacey et al. [32] have also reported a small shift of the IR bands of an EPR-silent CO-complex they called SI-CO at pH 6 and SI-CO_{red} at pH 9 (see Table 2). Using DFT they proposed that in the CO-complex the Ni(II) is high-spin and that in the SI-CO_{red} state a spin–spin interaction with the reduced proximal cluster is responsible for the small change in the FT-IR signal. However, the DFT model is significantly different from the crystallographic model of the CO-complex in the *D. vulgaris* (Miyazaki) enzyme [14] (Table 1). Consequently, it is not clear whether the distortion from square pyramidal coordination observed in the crystal is high enough to stabilize a high spin Ni(II). The relatively high vibration frequency of the bound exogenous CO [32,38], which suggests a not very tight terminal ligation mode, agrees very well with the bent binding mode observed by crystallography and deduced from resonance Raman spectroscopy [14].

Both electron and proton exchange reactions are blocked in the SI-CO state. CO binding studies have also shown that only Ni-SI and Ni-C can react with CO [32]. In the other states, the Ni is probably coordination-saturated [47] and apparently CO cannot displace exogenous ligands, such as oxygen, from the active site. Also, in the more reduced Ni-C and Ni-R states simultaneous binding of H^- and CO does not take place because of a competition between the two ligands [32]. The Ni-C state is obtained by reducing hydrogenase with H_2 in the absence of inhibitors such as O_2 and CO. Under these conditions, no traces of the Ni-SI states are observed. As in the SI-CO complex mentioned above, the IR frequencies characteristic of the Ni-C species underwent very small shifts when the pH was changed from 6 to 9 [40]. This may result, again, from the reduction of the proximal [4Fe–4S] cluster at pH 9, which generates the so-called split Ni-C EPR signal [21,48]. Redox titrations have indicated that the Ni-C state is most likely two electrons more reduced than Ni-B [49]. If these two states have Ni(III), the latter should bind H^- or H_2. Exposure of an active enzyme preparation to white light causes the disappearance of a proton hyperfine coupling as detected at very low temperature by ENDOR spectroscopy; it also generates another EPR signal called Ni-L [48]. This has been interpreted as the consequence of photolytic cleavage of a Ni-bound hydride [50]. Direct evidence for the presence of a bridging hydride in Ni-C has recently been obtained from ENDOR and four-pulse ESEEM measurements of the H_2-sensing hydrogenase from *Ralstonia eutropha* [51].

Very recent DFT analyses ([52] and references therein) show good agreement between calculated and observed EPR parameters for the Ni-C when it is modeled as a formal Ni(III) and a bridging hydride ligand (Fig. 3B). A DFT model of Ni-L where Ni is assigned the 1+ redox state is also in excellent agreement with EPR results at low temperature:

$$\text{Ni(III)–H}^- + h\nu \Rightarrow \text{Ni(I)} + \text{H}^+ \quad (2)$$

Careful examination of the IR frequencies also suggests the presence of a hydride in both Ni-C and Ni-R states. If frequency differences are calculated among the various states, it becomes evident that in certain cases the shifts of the CN and CO bands differ significantly. For instance, the differences between Ni-SI_{II} and Ni-C are (0, 0, 17) for the symmetrical and asymmetrical stretching frequencies of CN^- and for CO. The simplest explanation for this difference is the trans influence of H^- on the C–Fe bond of the CO ligand. Trans effects occur when two ligands share a metal orbital [53]. In [NiFe]-hydrogenases a bridging ligand would share the same dz^2 orbital of the Fe with CO. H^- has a strong trans influence: it preempts the orbital and makes the C–Fe bond weak which, in turn, strengthens the triple CO bond. Thus, although the active site is being reduced in going from Ni-SI_{II} to Ni-C, the CO frequency increases. Because the differences between Ni-C and the various Ni-R states are similar for CN^- and CO (see Table 2), the latter should also have a bridging hydride.

The EPR spectrum of a CO complex that is only stable at very low temperature can be closely mimicked by a Ni(I)-CO model using DFT [52]. It is also known that photolytic cleavage of the Ni-CO bond produces the Ni-L EPR spectrum [54]. However, the absence of a significant shift of the Ni absorption edge after the Ni-C to Ni-L transition does not agree with the two-electron reduction of Ni [34]. Overall, the spectroscopic results are consistent with the crystal structure of the CO complex of *D. vulgaris* (Miyazaki) [NiFe]-hydrogenase and its photosensitivity [14], although in that case diffraction data were collected at 100 K and the structure is likely to correspond to the EPR-silent SI-CO state resulting from the reaction:

$$\text{Ni(III)–H}^- + \text{CO} + [\text{4Fe–4S}]^{2+} \Rightarrow \text{Ni(II)–CO} + [\text{4Fe–4S}]^{+} + \text{H}^+ \quad (3)$$

The structural similarity between the photolyzed species and reduced enzyme (Table 1) suggests that the latter could correspond to the Ni-C state, resulting from the reverse of reaction (3). Alternatively, the photolytic cleavage of the nickel–carbon bond may have produced the Ni-SI_{II} state, as observed in FT-IR studies [38,39].

Bleijlevens et al. [40] detected three different sets of IR bands for the fully reduced Ni-R state (Table 2). The state with the highest frequencies was more abundant at low pH, whereas the state with the lowest frequencies was only detectable at high pH. These results suggest that three different protonation states are possible for Ni-R. Alternatively, frequency changes may also be due to different spin states: a DFT analysis of Ni-R models with a bridging hydride and either high or low spin Ni(II) [55] indicated that the latter model was quite close to the crystal structure of reduced enzyme, whereas the former was significantly different (Table 1). Nevertheless, there was a very small energy difference between the two states so both might be catalytically relevant.

2.4. Recent kinetic data

The first stopped-flow FT-IR studies of reactions of active and inactive [NiFe] *A. vinosum* hydrogenase preparations with H_2, CO and O_2 have been recently reported [43,56]. The redox state of the FeS clusters had to be included in the interpretation of the data, as these are involved in fast electron transfer to and from the active site. The ready Ni-B state activated rapidly upon H_2 addition with a lag time of 6 s [43]. The putative bridging hydroxide ligand of Ni-B was proposed to act as a base for the heterolytic cleavage of H_2, with electron transfer to the proximal FeS cluster and formation of a ready Ni-SI state:

$$\text{Ni(III)–OH}^- + \text{H}_2 + [\text{4Fe–4S}]^{2+} \Rightarrow \text{Ni(II)} + \text{H}_2\text{O} + [\text{4Fe–4S}]^{+} + \text{H}^+ \quad (4)$$

When a minor Ni-B fraction was activated with H_2 and then clamped in the inactive SI-CO state, the larger Ni-A fraction did not change after subsequent addition of H_2. When no CO was used, a slow transition from the Ni-A to the Ni-SU state was observed, which was ascribed to a one-electron transfer reaction from a small fraction of activated enzyme [43]. This experiment indicated that unready enzyme does not react with H_2. On the other hand, both Ni-SI_{II} and Ni-C states of the *A. vinosum* enzyme reacted with H_2 on a milli-second timescale, showing very high affinity for the substrate. For the former state, the reaction had to be performed at 25 °C or higher, whereas for the latter the proximal cluster had to be oxidized [56]:

$$\text{Ni(III)–H}^- + [\text{4Fe–4S}]^{2+} + \text{H}_2 \Rightarrow \text{Ni(II)–H}^- + [\text{4Fe–4S}]^{+} + 2\text{H}^+ \quad (5)$$

As already reported [49,57] (5) was the only reaction where hydrogen and the enzyme were at equilibrium. At pH 6, with an oxidized proximal cluster and in the absence of H_2, the Ni-C state remained stable for at least 1 day [56,58]. At pH 8 and in the absence of one-electron redox mediators, a slow transition from the Ni-C to the Ni-SI state was observed, compatible with the reaction:

$$\text{Ni(III)–H}^- + [\text{4Fe–4S}]^{+} + \text{H}^+ \Rightarrow \text{Ni(II)} + [\text{4Fe–4S}]^{2+} + \text{H}_2 \quad (6)$$

Reaction (6) was faster in the presence of redox mediators such as benzyl viologen and in the absence of H_2. However, the reaction was much slower than the Ni-R to Ni-C transition under similar conditions at lower potential. The reverse of reaction (6) probably explains the rapid H_2 binding at 25 °C to the active Ni-SI_{II} state. At 2 °C the Ni-SI_{II} was found to be in a ready (inactive) state and both CO and H_2 binding to this state was found to be very slow. The authors proposed that slow release of a trapped water molecule must occur prior to the binding of these gases [56].

The Ni-R state reacted very rapidly with CO, probably according to:

$$\text{Ni(II)–H}^- + \text{CO} + \text{H}^+ \Rightarrow \text{Ni(II)–CO} + \text{H}_2 \quad (7)$$

The Ni-C state reacted much more slowly, presumably according to reaction (3) indicating that, as expected from chemical considerations, CO binds faster to Ni(II) than to Ni(III). At first sight, these results seem to be in contradiction with those of De Lacey et al. [32], who found the Ni-R state to be stable in the presence of CO. This may be due to the fact that in their case a very low redox potential was maintained electrochemically.

A very powerful technique to study the kinetic processes is protein film voltammetry [8,44,47] (for a recent review the reader is referred to Lamle et al. [59]). The H_2 oxidation rate of a small amount of *A. vinosum* [NiFe]-hydrogenase adsorbed on a graphite electrode approached 10,000 s^{-1} at 45 °C, comparable to that of a Pt-coated electrode. It was concluded that the rate-limiting step is the diffusion of H_2 to the active site [60].

2.5. Proposed catalytic mechanisms

Using DFT models, it has been proposed that a structural water molecule is the base that accepts a proton upon the heterolytic splitting of H_2, which, in turn, generates a hydride in Ni-C [52]. However, this water was hydrogen-bonded to the two CN^- ligands of the active site iron, a proposition that is not stereochemically feasible. In addition, there is no indication of a water molecule in the vicinity of the active site in any of the reduced [NiFe] hydrogenase structures. No traces of any Ni-SI state have been observed under H_2 [40], suggesting that it may not be involved in catalysis and that the formation of the Ni-C state is part of the activation process of the enzyme.

The terminal Ni binding site occupied by CO in the inhibited enzyme has been proposed to be also the site of initial H_2 activation [14]. In the 1.2 Å resolution Fourier map of a CO complex, unexplained electron density was found at bonding distance from Cys530S. Ogata et al. suggested that this density is part of a trapped intermediate, maybe a protonated

species. This proton could have originated from the putative bridging hydride upon reaction of the crystalline Ni-C form with CO (see reaction (3)). The S_γ-atom of Cys530 and the side chain of Glu18 show relative high B-factors. These are a measure of discrete and/or dynamic disorder in a crystal structure, suggesting that these residues can adopt more than one conformation and protonation state. Besides playing a role in the formation of the Ni-B species, Glu18 is also likely to be involved in proton transfer; its mutation to glutamine abolishes both hydrogen turnover and H/D exchange [46].

In vivo, both Ni-SI_{II} and Ni-C forms of hydrogenase may react with hydrogen depending on temperature and overall redox state. Binding of hydrogen to either state will generate one of the N-R species, although the mechanism would not be exactly the same. Initially, the Ni-SI_{II} to Ni-R transition should involve the heterolytic cleavage of H_2, generation of a bridging hydride and re-oxidation to the Ni-C state by transfer of one electron to an oxidized [4Fe–4S] cluster, according to the reverse of reaction (6). After this step, catalysis will continue through the binding of H_2 to the terminal Ni binding site of the Ni-C state, possibly triggering the transient formation of a Ni-L-like state by transfer of a proton (the former bridging hydride) to Cys530 and reduction of Ni(III) to Ni(I) (reaction (2)). Subsequently, one electron from Ni and the proton from Cys530 would be transferred to the proximal cluster. After heterolytic cleavage the resulting hydride could move to the vacant Ni–Fe bridging position (see reaction (5)). Alternatively, H_2 could move to the bridging site, get polarized between Fe and Ni and then be heterolytically cleaved. Thus, there are several candidates for the base that would initially bind the proton generated by the first part of reaction (1). One can even conceive that it is the bridging hydride in the Ni-C state that abstracts a proton from H_2. In that case one electron from a transient terminally bound hydride would bind the Ni ion generating the Ni-R state; the other electron and one proton would be transferred to the proximal cluster.

Hydride binding to a FeCOCN unit following the heterolytic cleavage of H_2 has also been postulated in Fe-only hydrogenases [61].

Fraser Armstrong has remarked that, given the high activity of [NiFe]-hydrogenases, it is doubtful that all spectroscopically observed active enzyme states are catalytic intermediates [8]. This situation complicates the interpretation and it is clear that additional studies will be needed in order to improve our understanding of the catalytic mechanism of these fascinating enzymes.

3. Structural comparisons with CODH and ACS

Carbon monoxide dehydrogenase (CODH) and acetyl coenzyme A synthase (ACS) are found in many anaerobic microorganisms that use the anaerobic Wood–Ljungdahl pathway of acetyl CoA synthesis [62]. CODH reduces CO_2 to CO according to the reaction:

$$CO_2 + H^+ + 2e^- \Rightarrow CO + OH^- \quad (8)$$

ACS combines the produced CO molecule with a methyl group according to the reaction:

$$CO + CH_3{}^+ + CoA\text{-}S^- \Rightarrow CoA\text{-}SC(O)CH_3 \quad (9)$$

The methyl group originates from the reduction of a second CO_2 molecule and is transferred to ACS by a cobalt-containing corrinoid iron–sulfur protein (CFeSP). In acetogens like *Moorella* (*M.*) *thermoacetica*, the ACS (α-subunit) and the CODH (β-subunit) form $\alpha_2\beta_2$ heterotetramers [63]. Both enzymes are also found in methanogens where they function in a reverse pathway that generates low potential electrons from acetyl-CoA by decarbonylation of the acetyl group and oxidation of the resulting CO to CO_2 [64]. They are associated with three other protein subunits γδε, where γδ corresponds to CFeSP, in a $(\alpha\beta\gamma\delta\varepsilon)_8$ multi-enzyme complex [65]. Isolated homodimeric CODHs have been characterized in *Carboxidothermus* (*C.*) *hydrogenoformans* [66] and *Rhodospirillum* (*R.*) *rubrum* [67]. By catalyzing the reverse of reaction (8) they allow these organisms to use CO as sole carbon and energy source.

A number of recent reviews have addressed the abundant spectroscopic and kinetic data on CODH and ACS [64,68–72]. Here we will focus on the structural information obtained in the last few years. Two crystal structures of CODH, from *C. hydrogenoformans* and *R. rubrum*, were reported in 2001 at 1.6 and 2.8 Å resolution, respectively [66,67]. They showed that the CODH dimer contains two B-clusters and two C-clusters, as expected from spectroscopic data. Surprisingly, another cluster called D was found at the dimer interface. The B and D clusters are regular [4Fe–4S] cubanes that provide an electron transfer pathway between the molecular surface and the Ni-containing C-cluster. The latter constitutes the active site and consists of a [3Fe–4S] sub-site that is connected to a Ni and a unique Fe ion called ferrous component II (FCII) via three of its inorganic S-atoms (Fig. 4a). An almost identical CODH dimer was subsequently found in two crystal structures of the CODH/ACS complex of *M. thermoacetica* (Fig. 1B) [63,73].

In all the CODH structures, the B-factors of the C-cluster atoms are rather high. This indicates that the C-cluster is either partially occupied, as found for the *C. hydrogenoformans* enzyme [66] or present in more than one conformation, as reported for the 1.9 Å resolution crystal structure of the CO complex of the *M. thermoacetica* enzyme [73]. Significant differences are apparent between the four reported C-cluster structures and they will be discussed elsewhere. The C-cluster has two cis Ni binding sites available for exogenous ligands, here called E1 and E2. E2 bridges the Ni ion and FCII and in the *C. hydrogenoformans* structure it is occupied by a fifth labile sulfide [66]. This ligand may arise from the reduction of COS, which is an alternative substrate of CODH [74]:

$$COS + H^+ + 2e^- \Rightarrow CO + SH^- \quad (10)$$

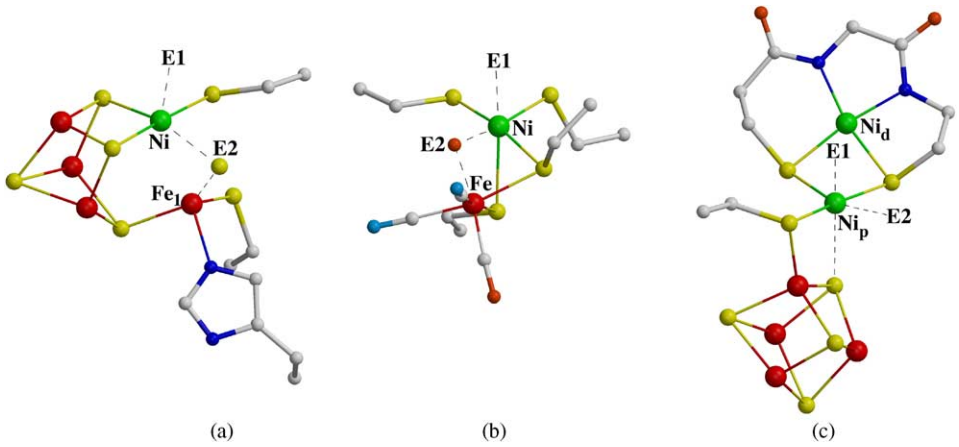

Fig. 4. Comparison of Ni–Fe active sites of (a) CODH, (b) hydrogenase and (c) ACS.

Thus, the hydroxide produced by reaction (8) could also occupy a Ni–Fe bridging position prior to its protonation and release as a water molecule. CO may bind to E1, as suggested by the structure of the CO-complex of the *M. thermoacetica* enzyme [73]. In a more recent report concerning CODH from *C. hydrogenoformans*, it was found that treating the enzyme with excess CO results in the absence of a labile sulfide at E2 but also in the loss of enzymatic activity [75]. This suggested that E2 is permanently occupied by an S-atom. However, such a structure would not provide the two open cis coordination sites to the Ni that are most likely required to bind CO and OH^-, products of the two-electron reduction of CO_2. Furthermore, in a recent paper Feng and Lindahl have shown that incubating CODH from either *M. thermoacetica* or *R. rubrum* with Na_2S inhibits the catalytic activity [76] and modifies the EPR spectrum of the C-cluster. Removal of S^{2-} restores the catalytic activity. Based on these results, the authors suggested that SH^- occupies the E2 site, as seen in the *C. hydrogenoformans* CODH crystal structure.

The 2.2 Å resolution structure of ACS/CODH$_{Mt}$ revealed the presence of an extensive hydrophobic tunnel network connecting the four active sites, i.e. the two A- and C-clusters of the heterotetramer (Fig. 1) [63]. The CO produced at the C-cluster is thought to diffuse through the tunnels to the A-cluster because under normal turnover conditions no CO escapes from the enzyme [77,78]. Moreover, the acetylation of CoA is more effective when using CO_2 plus reductant than with CO provided from the medium [78]. In fact, CO is probably never an external substrate in ACS/CODHs [79]. The 1.9 Å resolution structure of another crystal form of the same enzyme showed that ACS, which is composed of three globular domains, may adopt closed and open conformations [73]. In the former, the A-cluster is relatively inaccessible but connects to the C-cluster by the hydrophobic tunnel, whereas in the latter the A-cluster lies exposed at the molecular surface and the tunnel is blocked (Fig. 1B). Recently, the structure of a monomeric ACS of *C. hydrogenoformans* has also been solved in an open domain conformation [80]. We have proposed that the observed conformational changes of ACS are important for the correct gating of substrates and products at the A cluster [73,81]. So far, three metal compositions have been found for the active site A-cluster: Fe_4S_4CuNi [63], Fe_4S_4ZnNi [73] and Fe_4S_4NiNi [73,80]. It is now widely accepted that the Fe_4S_4NiNi structure is the only active one (Fig. 4c). The distal Ni ion (with respect to the FeS cluster) is called Ni$_d$ and is probably catalytically inert. The proximal Ni$_p$ is thought to be the catalytic center because it is more accessible to solvent and has two cis coordination sites (again labeled E1 and E2) available for CO and CH_3 binding (see reaction (9)). In the closed ACS conformation, E1 points to the exit of the long hydrophobic tunnel so this is most likely where CO binds. In the open conformation, E2 becomes very exposed to the solvent, making it the best candidate to accept the methyl group from the bulky CFeSP. More structural evidence is clearly needed to confirm this.

In the two *M. thermoacetica* structures, the C-cluster has no visible ligand at the E2 position, leaving FCII with apparently only three ligands. One possibility is that E2 binds a hydride, which would make it similar to the proposed bridging hydride site in the active states of [NiFe] hydrogenase. The hydride could react with CO_2 bound to the E1 site, producing a CO at E1 and an OH^- at E2 (reaction (10)). Because of the already mentioned heterogeneity at the C-cluster in the different crystal structures, data from more homogenous samples will be needed to improve our understanding of the catalytic mechanism at the C-cluster.

4. Conclusion

In summary, the active site structures of CODH, ACS and [NiFe]-hydrogenase show several common features. They act on gaseous substrates and they all contain a Ni–Fe pair with the Ni located near the exit of a long hydrophobic tunnel. In each case, the catalytic Ni ion has two open cis coordination sites, E1 and E2, available for substrate binding. E1 points at the tunnel and binds CO in [NiFe]-hydrogenase [14] and CODH [74]. For mechanistic and stereochemical reasons

E1 is also very likely the CO binding site in the A-cluster [73,81]. E2 has been postulated to bind a hydride in [NiFe]-hydrogenase [51] and it might also bind H^- in the C-cluster of CODH. In both [NiFe]-hydrogenase and CODH, an inorganic S-atom has been found at the Ni-Fe bridging site [12,66], which further indicates that the two active sites have remarkably similar properties. What is missing in CODH is the presence of structural CO and CN ligands to the Fe, which might explain why it does not function as a very effective hydrogenase: only a low hydrogen evolution activity has been reported for this enzyme [82]. In the A-cluster, E2 is a terminal coordination site thought to bind CH_3.

The association of Ni, Fe and S has been shown to have interesting catalytic properties even in an abiotic context. In enzymes, NiFe-containing clusters are involved in reactions that provide reducing power and, in the case of CODH, a carbon source, from very simple molecules such as CO and H_2. These gases, along with CO_2, were very abundant in the early history of earth and it is almost certain that they were extensively used by primitive anaerobic microorganisms. At present, the required anoxic environments are confined to a few niches. Nevertheless, relatives of ancestral bacteria and archaea continue to thrive there, carrying out fascinating chemical reactions that we are just beginning to understand.

Acknowledgements

This work was supported by the CEA, the CNRS and by the European Union BIOTECH Program, grant BIO4-98-0280.

References

[1] M.J. Russell, W. Martin, Trends Biochem. Sci. 29 (2004) 358.
[2] C. Huber, G. Wächtershäuser, Science 281 (1998) 670.
[3] M. Frey, J.C. Fontecilla-Camps, A. Volbeda, in: A. Messerschmidt, R. Huber, T. Poulos, K. Wieghardt (Eds.), Handbook of Metalloproteins, 2, Wiley, Chichester, UK, 2001, p. 880.
[4] R. Cammack, R. Robson, M. Frey (Eds.), Hydrogen as a Fuel, Learning from Nature, Taylor & Francis, London, 2001.
[5] P.M. Vignais, B. Billoud, J. Meyer, FEMS Microbiol. Rev. 25 (2001) 455.
[6] S.P.J. Albracht, in: L.G. Ljungdahl (Ed.), Biochemistry and Physiology of Anaerobic Bacteria, Springer-Verlag, New York, 2003, p. 20.
[7] A. Volbeda, J.C. Fontecilla-Camps, Dalton Trans. (2003) 4030.
[8] F.A. Armstrong, Curr. Opin. Chem. Biol. 8 (2004) 133.
[9] P.M. Vignais, A. Colbeau, Curr. Issues Mol. Biol. 6 (2004) 159.
[10] A. Volbeda, M.H. Charon, C. Piras, E.C. Hatchikian, M. Frey, J.C. Fontecilla-Camps, Nature 373 (1995) 580.
[11] A. Volbeda, E. Garcin, C. Piras, A.L. De Lacey, V.M. Fernandez, E.C. Hatchikian, M. Frey, J.C. Fontecilla-Camps, J. Am. Chem. Soc. 118 (1996) 12989.
[12] Y. Higuchi, T. Yagi, N. Yasuoka, Structure 5 (1997) 1671.
[13] Y. Higuchi, H. Ogata, K. Miki, N. Yasuoka, T. Yagi, Structure 7 (1999) 549.
[14] H. Ogata, Y. Mizoguchi, N. Mizuno, K. Miki, S. Adachi, N. Yasuoka, T. Yagi, O. Yamauchi, S. Hirota, U. Higuchi, J. Am. Chem. Soc. 124 (2002) 11628.
[15] Y. Montet, P. Amara, A. Volbeda, X. Vernede, E.C. Hatchikian, M.J. Field, M. Frey, J.C. Fontecilla-Camps, Nat. Struct. Biol. 4 (1997) 523.
[16] A. Volbeda, Y. Montet, X. Vernède, E.C. Hatchikian, J.C. Fontecilla-Camps, Int. J. Hydrogen Energy 27 (2002) 1449.
[17] P.M. Matias, C.M. Soares, L.M. Saraiva, R. Coelho, J. Morais, J. Le Gall, M.A. Carrondo, J. Biol. Inorg. Chem. 6 (2001) 63.
[18] E. Garcin, X. Vernède, E.C. Hatchikian, A. Volbeda, M. Frey, J.C. Fontecilla-Camps, Structure 7 (1999) 557.
[19] Y. Nicolet, B.J. Lemon, J.C. Fontecilla-Camps, J.W. Peters, Trends Biochem. Sci. 25 (2000) 138.
[20] S. Reissmann, E. Hochleitner, H. Wang, A. Paschos, F. Lottspeich, R.S. Glass, A. Bock, Science 299 (2003) 1067.
[21] R. Cammack, D.S. Patil, E.C. Hatchikian, V.M. Fernandez, Biochim. Biophys. Acta 912 (1987) 98.
[22] V.M. Fernandez, E.C. Hatchikian, R. Cammack, Biochim. Biophys. Acta 832 (1985) 69.
[23] V.M. Fernandez, E.C. Hatchikian, D.S. Patil, R. Cammack, Biochim. Biophys. Acta 883 (1986) 145.
[24] J.C. Salerno, in: J.R. Lancaster (Ed.), The Bioinorganic Chemistry of Nickel, VCH, Weinheim, FRG, 1988, p. 53.
[25] O. Trofanchuk, M. Stein, C. Geßner, F. Lendzian, Y. Higuchi, W. Lubitz, J. Biol. Inorg. Chem. 5 (2000) 36.
[26] R.P. Happe, W. Roseboom, A.J. Pierik, S.P.J. Albracht, K.A. Bagley, Nature 385 (1997) 126.
[27] A.L. De Lacey, E.C. Hatchikian, A. Volbeda, M. Frey, J.C. Fontecilla-Camps, V.M. Fernandez, J. Am. Chem. Soc. 119 (1997) 7181.
[28] A.J. Pierik, W. Roseboom, R.P. Happe, K.A. Bagley, S.P.J. Albracht, J. Biol. Chem. 274 (1999) 3331.
[29] D.J. Darensbourg, J.H. Reibenspies, C.-H. Lai, W.-Z. Lee, M.Y. Darensbourg, J. Am. Chem. Soc. 119 (1997) 7903.
[30] S. Niu, L.M. Thomson, M.B. Hall, J. Am. Chem. Soc. 121 (1999) 4000.
[31] P. Amara, A. Volbeda, J.C. Fontecilla-Camps, M.J. Field, J Am Chem Soc 121 (1999) 4468.
[32] A.L. De Lacey, C. Stadler, V.M. Fernandez, E.C. Hatchikian, H.-J. Fan, S. Li, M.B. Hall, J. Biol. Inorg. Chem. 7 (2002) 318.
[33] Z. Gu, J. Dong, C.B. Allan, S.B. Choudhury, R. Franco, J.J.G. Moura, I. Moura, J. LeGall, A.E. Przybyla, W. Roseboom, S.P.J. Albracht, M.J. Axley, R.A. Scott, M.J. Maroney, J. Am. Chem. Soc. 118 (1996) 11155.
[34] G. Davidson, S.B. Choudhury, Z. Gu, K. Bose, W. Roseboom, S.P.J. Albracht, M.J. Maroney, Biochemistry 39 (2000) 7468.
[35] M.J. Maroney, P.A. Bryngelson, J. Biol. Inorg. Chem. 6 (2001) 453.
[36] W. Gu, L. Jacquamet, D.S. Patil, H.X. Wang, D.J. Evans, M. Millar, S. Koch, D.M. Eichhorn, M. Latimer, S.P. Cramer, J. Inorg. Biochem. 93 (2003) 41.
[37] S.P.J. Albracht, Biochim. Biophys. Acta 1188 (1994) 167.
[38] K.A. Bagley, C.J. van Garderen, M. Chen, E.C. Duin, S.P.J. Albracht, W.H. Woodruff, Biochemistry 33 (1994) 9229.
[39] K.A. Bagley, E.C. Duin, W. Roseboom, S.P.J. Albracht, W.H. Woodruff, Biochemistry 34 (1995) 5527.
[40] B. Bleijlevens, F.A. van Broekhuizen, A.L. De Lacey, W. Roseboom, V.M. Fernandez, S.P.J. Albracht, J. Biol. Inorg. Chem. 9 (2004) 743.
[41] M. Stein, E. Van Lenthe, E.J. Baerends, W. Lubitz, J. Am. Chem. Soc. 123 (2001) 5839.
[42] C. Stadler, A.L. De Lacey, Y. Montet, A. Volbeda, J.C. Fontecilla-Camps, J. Conesa, V.M. Fernandez, Inorg. Chem. 41 (2002) 4424.
[43] S. Kurkin, S.J. George, R.N. Thorneley, S.P. Albracht, Biochemistry 43 (2004) 6820.
[44] A.K. Jones, S.E. Lamle, H.R. Pershad, K.A. Vincent, S.P.J. Albracht, F.A. Armstrong, J. Am. Chem. Soc. 125 (2003) 8505.

[45] A.L. De Lacey, A. Pardo, V.M. Fernandez, S. Dementin, G. Adryanczyk-Perrier, E.C. Hatchikian, M. Rousset, J. Biol. Inorg. Chem. 9 (2004) 636.
[46] S. Dementin, B. Burlat, A.L. De Lacey, A. Pardo, G. Adryanczyk-Perrier, B. Guigliarelli, V.M. Fernandez, M. Rousset, J. Biol. Chem. 279 (2004) 10508.
[47] C. Leger, S. Dementin, P. Bertrand, M. Rousset, B. Guigliarelli, J. Am. Chem. Soc. 126 (2004) 12162.
[48] F. Dole, M. Medina, C. More, R. Cammack, P. Bertrand, B. Guigliarelli, Biochemistry 35 (1996) 16399.
[49] L.M. Roberts, P.A. Lindahl, J. Am. Chem. Soc. 117 (1995) 2565.
[50] J.P. Whitehead, R.J. Gurbiel, C. Bagyinka, B.M. Hoffman, M.J. Maroney, J. Am. Chem. Soc. 115 (1993) 5629.
[51] M. Brecht, M. van Gastel, T. Buhrke, B. Friedrich, W. Lubitz, J. Am. Chem. Soc. 125 (2003) 13075.
[52] M. Stein, W. Lubitz, J. Inorg. Biochem. 98 (2004) 862.
[53] F.A. Cotton, G. Wilkinson, Advanced Inorganic Chemistry, 5th ed., Wiley, 1988, p. 1299.
[54] J.W. van der Zwaan, S.P.J. Albracht, R.D. Fontijn, Y.B.M. Roelofs, Biochim. Biophys. Acta 872 (1986) 208.
[55] M. Bruschi, L. De Gioia, G. Zampella, M. Reiher, P. Fantucci, M. Stein, J. Biol. Inorg. Chem. 9 (2004) 873.
[56] S.J. George, S. Kurkin, R.N. Thorneley, S.P. Albracht, Biochemistry 43 (2004) 6808.
[57] J.M. Coremans, J.W. van der Zwaan, S.P. Albracht, Biochim. Biophys. Acta 1119 (1992) 157.
[58] D.P. Barondeau, L.M. Roberts, P.A. Lindahl, J. Am. Chem. Soc. 116 (1994) 3442.
[59] S.E. Lamle, K.A. Vincent, L.M. Halliwell, S.P.J. Albracht, F.A. Armstrong, Dalton Trans. (2003) 4152.
[60] A.K. Jones, E. Sillery, S.P.J. Albracht, F.A. Armstrong, Chem. Commun. (2002) 866.
[61] Y. Nicolet, A.L. De Lacey, X. Vernède, V.M. Fernandez, E.C. Hatchikian, J.C. Fontecilla-Camps, J. Am. Chem. Soc. 123 (2001) 1596.
[62] H.G. Wood, FASEB J. 5 (1991) 156.
[63] T.I. Doukov, T.M. Iverson, J. Seravalli, S.W. Ragsdale, C.L. Drennan, Science 298 (2002) 567.
[64] D.A. Grahame, Trends Biochem. Sci. 28 (2003) 221.
[65] B. Bhaskar, E. DeMoll, D.A. Grahame, Biochemistry 37 (1998) 14491.
[66] H. Dobbek, V. Svetlitchnyi, L. Gremer, R. Huber, O. Meyer, Science 293 (2001) 1281.
[67] C.L. Drennan, J. Heo, M.D. Sintchak, E. Schreiter, P.W. Ludden, Proc. Natl. Acad. Sci. U.S.A. 98 (2001) 11973.
[68] P.A. Lindahl, Biochemistry 41 (2002) 2097.
[69] C.G. Riordan, J. Biol. Inorg. Chem. 9 (2004) 509.
[70] P.A. Lindahl, J. Biol. Inorg. Chem. 9 (2004) 516.
[71] T.C. Brunold, J. Biol. Inorg. Chem. 9 (2004) 533.
[72] E.L. Hegg, Acc. Chem. Res. 37 (2004) 775.
[73] C. Darnault, A. Volbeda, E.J. Kim, P. Legrand, X. Vernède, P.A. Lindahl, J.C. Fontecilla-Camps, Nat. Struct. Biol. 10 (2003) 271.
[74] S.A. Ensign, Biochemistry 34 (1995) 5372.
[75] H. Dobbek, V. Svetlitchnyi, J. Liss, O. Meyer, J. Am. Chem. Soc. 126 (2004) 5382.
[76] J. Feng, P.A. Lindahl, J. Am. Chem. Soc. 126 (2004) 9094.
[77] E.L. Maynard, P.A. Lindahl, J. Am. Chem. Soc. 121 (1999) 9221.
[78] J. Seravalli, S.W. Ragsdale, Biochemistry 39 (2000) 1274.
[79] D.A. Grahame, E. DeMoll, Biochemistry 34 (1995) 4617.
[80] V. Svetlitchnyi, H. Dobbek, W. Meyer-Klaucke, T. Meins, B. Thiele, P. Romer, R. Huber, O. Meyer, Proc. Natl. Acad. Sci. U.S.A. 101 (2004) 446.
[81] A. Volbeda, J.C. Fontecilla-Camps, J. Biol. Inorg. Chem. 9 (2004) 525.
[82] S. Menon, S.W. Ragsdale, Biochemistry 35 (1995) 15814.